Asian Journal of Chemistry; Vol. 25, No. 17 (2013), 9460-9464

ASIAN JOURNAL OF CHEMISTRY

http://dx.doi.org/10.14233/ajchem.2013.15025

Theoretical Study of Catalytic Reaction Mechanism of CO with N_2O by Cu^+

DONG-PING CHEN[1,*], KE GAI[1], CHAO KONG[2], YAN-XIA HAN[1], LI-JIE HOU[1] and BO-WANG WU[1]

[1]College of Chemistry and Chemical Engineering, Longdong University, Qingyang 745000, Gansu Province, P.R. China
[2]Lanzhou Institute of Chemical Physics, University of Chinese Academy of Sciences, Lanzhou 730000, Gansu Province, P.R. China

*Corresponding author: Tel: +86 18393820120; E-mail: tswscdp@163.com

(*Received*: 26 December 2012; *Accepted*: 1 October 2013) AJC-14205

The entire reaction mechanism for the gas-phase $CO(C_{\infty v},{}^1\Sigma^+) + N_2O(C_{\infty v},{}^1\Sigma) \rightarrow N_2(D_{\infty h},{}^1\Sigma^+_g) + CO_2(D_{\infty h},{}^1\Sigma_g^+)$ catalytic reaction by the bare Cu^+ are discussed by the density function theory(DFT). The calculated results explicitly indicated that the reaction exist spin-forbidden phenomenon between the singlet and the triplet potential energy surfaces (PESs). Two crossing points (CP1 and CP2) which play a significant role in this catalytic reaction. The values of the spin-orbit coupling constants are 673.1 cm^{-1} at CP1 and 284.2 cm^{-1} at CP2, which indicate that the spin crossing process can occur efficiently due to the large spin-orbit coupling involved. This process made the value of activation energy reduce 108.5 kJ/mol, which are helpful for the reaction on kinetics and thermodynamics.

Key Words: Cu^+, Reaction mechanism, Density functional theory, Spin-orbit coupling.

INTRODUCTION

N_2O gives rise to nitric oxide which is responsible for the depletion of the ozone layer. Carbon monoxide is a significant toxic gas. How to reduce the environmental pollution resulted from N_2O and CO, which has been a hot subject for many experiments and theoretical calculations. The catalytic reactions mechanism of CO with N_2O by Fe^+, $Co^+$and Ni^+ were systematically investigated on potential energy surface using the quantum chemistry density functional theory[1-4]. Their research showed one oxygen atom of N_2O was directly extracted by metal ions to format metal oxide ion, there does not insertion of NO in reaction process. The reactions mechanism of N_2O with Ge^+ and Se^+ are directly extract oxygen mechanism using B3LYP/SDD+6-311+G(d) method by Chiodo *et al.*[5]. Additionally, the catalytic reactions mechanism of N_2O with CO by Pt^+ and CO with NO_2 by Sc^+ were investigated using density functional method[6,7]. Spin forbidden is an important factor to influence the reaction rate in gas phase reaction[5]. Many metal ions catalytic effect are not ideal because there is crossing and spin forbidden in different potential energy surfaces in reaction. The reactions of Ti^+ (^2F and ^4F) with N_2O and Cu^+ (^1S and ^4D) with N_2O were studied by Wang *et al.*[8,9]. They confirmed crossing phenomenon were existed in the export of reactions by research the potential energy surfaces of multiple states.

Recently, Böhme *et al.*[10] paid particular attention to the catalytic reactions of $CO(C_{\infty v},{}^1\Sigma^+) + N_2O(C_{\infty v},{}^1\Sigma) \rightarrow N_2(D_{\infty h},{}^1\Sigma^+_g) + CO_2(D_{\infty h},{}^1\Sigma_g^+)$ by transition metal ions in the gas phase. Experimental measurements carried out by using an inductively coupled plasma/selected-ion ow tube (ICP/SIFT) tandem mass spectrometer, tested the efficiency of many atomic cations to catalyze the reactions of nitrous oxide with carbon monoxide[10-12]. While the experimental procedure and the rate coefficients for this kind of O-atom transport reactions are well-known. Few theoretical investigations were performed to compute the potential energy surfaces (PES) for the catalytic cycle, illustrated in **Scheme-I**. So far, 26 atomic cations were experimentally checked for their catalytic performance, but only ten activate nitrous oxide at room temperature[11].

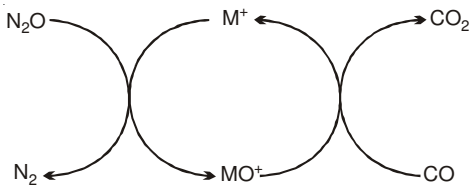

Scheme-I

In our work, we investigated the catalytic efficiency of Cu^+ by the theoretical study of the potential energy surface, which provide an explanation for its O-atom transfer reactivity. Cu^+ reacts sufficiently with N_2O to establish large enough concentrations of CuO^+ to obtain meaningful results for its reaction under experimental conditions with $k = 5.7 \times 10^{-13}$ cm^3 $molecule^{-1}$ s^{-1}, but for the CuO^+ with CO the measured shown the rate coefficient could not be measured because CuO^+ could not be established in sufficient amounts[10].

In this paper we will report the detailed mechanisms of the reactions Cu/N_2O/CO by using DFT. Calculated results are expected to check experimental findings and to give new suggestions that could not be reached experimentally under the considered conditions.

COMPUTATIONAL METHOD

The calculations were performed using the Gaussian03 program package[13]. At the indicated levels of theory, full geometry optimizations and frequency calculations were performed to verify the nature of the minima and evaluate zero-point energies. The fully optimized geometries and the vibrational frequencies have been determined using the spin-unrestricted three-parameter hybrid[14] B3LYP density method[15] and a standardized 6-311G basis set was used together with polarization (2d) and diffuse (+) function[16]. All stationary points are characterized by vibrations are included. The transition state structures all represent saddle points, characterized by one negative eigenvalue of the hessian matrix. To ensure the reliability of the reaction path, the pathways between the transition structures and their corresponding minima have been characterized by the internal reaction coordinate (IRC) calculations[17,18].

The natural population analysis had been made by using the natural bond orbital (NBO)[19] option as implemented in Gaussian 03.

In order to locate the crossing points (CPs) between the two potential energy surfaces (PESs) of different spin states, the procedure used by Heinemann *et al.*[20] was selected. We performed single-point energy calculations of the septet state as a function of the structural change along the IRC of the quintet state and *vice versa*[21,22].

Since in the case of the nickel catalyzed reaction we were interested also in the spin-orbit coupling (SOC) interaction which lend approximate one-electron spin-orbit coupling calculations have been carried out with the GAMESS[23] suit of programs in the version of 2007, using the effective one-electron SO operator[24], in the following equation:

$$H_{SO} = \frac{a^2}{2}\sum_i\sum_k\left(\frac{Z_K^*}{r_{jk}^3}\right)(S_i \times L_{ik}) = \sum_i h_i(Z^*)\frac{a^2}{2} = \frac{e^2h}{4\pi m_e^2 c^2}$$

where L_{ik} and S_i are the orbital and spin angular momentum operators for an electron i in the framework of the nuclei, indexed by K. To account for the missing two-electron part of the Hamiltonian,the nuclear charge Z_K is replaced by an effective parameter, Z_K^*, which can be taken as the screened nuclear charge.

RESULTS AND DISCUSSION

Overall of the stationary points: The optimized geometries for the stationary points at both the singlet and the triplet electronic states are depicted in Fig. 1, transition vectors are shown with arrows in the TS structures. Fig. 2 shows the schematic reaction mechanism with the relative energies of the reactants, intermediates species, TSs and products obtained at UB3LYP level. For all cited single-point energies are performed with UB3LYP/6-311++G(3df,3pd), zero-point energy (ZPE) corrections are included.

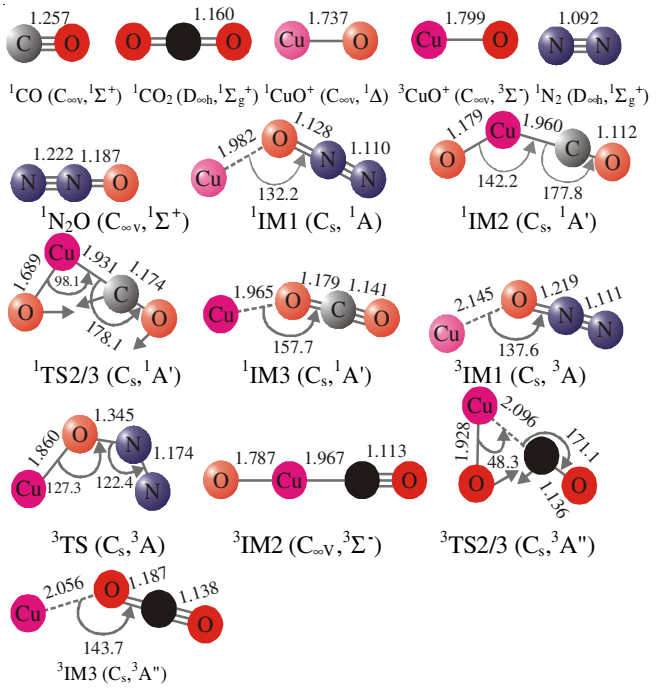

Fig. 1. Optimized geometries of various species in reaction. (bond length in Å, bond angles in degree)

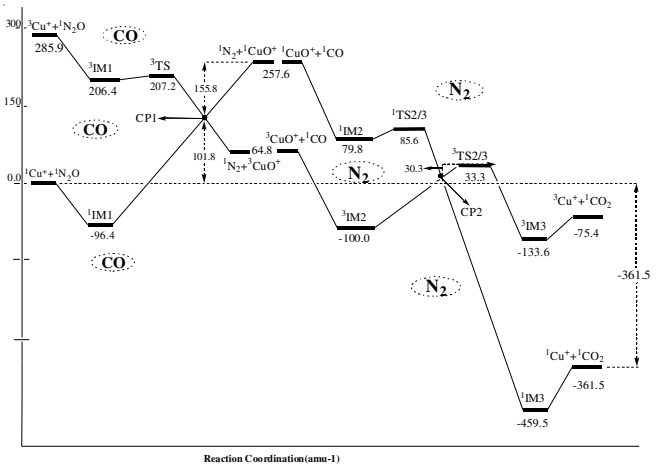

Fig. 2. Diagram of PESs for the reaction on the both spin states

There distinctly corresponsive courses are as follows: when Cu^+ reacts with N_2O, depending on the orientation of the approaching N_2O with respect to Cu^+. Firstly, attack *via* O leads to format CuO^+ and N_2. Secondly, attack *via* N-end leads to format CuN_2^+ and O atom. Finally, Cu^+ in the ^{3}D state can also reacts with N_2O *via* the central nitrogen to insert the bond of O-N_2(N_2 indicates the second N atom, the others are the same means) to format $[OCuNN]^+$[25]. In this paper, we mainly discussed this reaction course of O-end attack, because $[OCuNN]^+$ and CuN_2^+ have no catalytic performance. As shown in Figs. 1 and 2, Cu^+ attack the N_2O on the O-end to form the corresponding $[Cu\text{-}ONN]^+$ complexes ^{1}IM1 and ^{3}IM1 for singlet and triplet states. The first intermediate ^{1}IM1 and ^{3}IM1 structures are planar (C_s symmetry) and electronic states are ^{1}A and ^{3}A. Along the reaction pathway, ^{1}IM1 direct divided into $^1CuO^+$ and N_2, ^{3}IM1 convert into products $^3CuO^+$ and N_2 by ^{3}TS. $^1CuO^+$ and $^3CuO^+$ attack the C-end of CO to form the corresponds ^{1}IM2 and ^{3}IM2. ^{1}IM2 and ^{3}IM2 convert the ^{1}IM3

and ^{3}IM3 *via* an important transition structure ^{1}TS2/3 and ^{3}TS2/3, respectively. ^{1}IM3 and ^{3}IM3 can be viewed as product complexes which separated Cu^+ and CO_2.

Reaction mechanism

Calculation of the O-atom affinities: From the potential energy diagram of the reaction in Fig. 2 (**Scheme-I**), it can be showed that an important role was played by metal cation Cu^+ in the reaction of N_2O ($^1\Sigma^+$) + CO ($^1\Sigma^+$) ⟶ $N_2(^1\Sigma_g^+)$ + $CO_2(^1\Sigma_g^+)$ catalytic action. We may conclude that this reaction relates to metal cation's ability of O capture. To depict the ability of O capture, the O-atom affinities (OA) of Cu^+ is defined as follow: $OA(Cu^+) = IE(Cu) + D_{298}(Cu\text{-}O) - IE(CuO)$, which consults the method in the ion-molecule reactions of Cu^+ and CuO^+ in **Scheme-II**[26]:

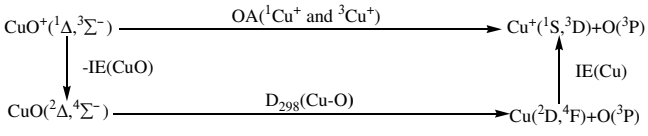

Scheme-II

The results in two spin states show in follow: OA ($^1Cu^+$) = 204.5 kJ mol^{-1}, OA ($^3Cu^+$) = 451.9 kJ mol^{-1}, OA (ON) = 197.0 kJ mol^{-1} and OA (CO) = 527.5 kJ mol^{-1}. Thus in high spin state and low spin state OA (Cu^+) are larger OA (ON) and less than OA (CO). This shows that Cu^+ can captures O atom from N_2O to give CuO^+ and CuO^+ transfers difficultly the oxygen atom to CO to produce CO_2 and Cu^+. Furthermore, the calculated OA ($^1Cu^+$) and OA (ON) energy are a small larger than the experimental value (156.5 ± 14.6 and 167.2 ± 0.08 kJ mol^{-1}) and the calculated OA (CO) energy is a small little than the experimental value (532.6 ± 0.08 kJ mol^{-1})[10]. This shows that the calculated results are in good agreement experimental values. All in all, the conclusion about the entire reaction mechanism that we have drawn is credible.

Orbital aspects: An analysis of molecular orbital at the UB3LYP/6-311+G(2d) level reveals the important orbital interactions at the initial complexes, which are shown in Figs. 3 and 4. The molecular orbital of N_2O show that the HOMO is a 2π bond orbit which is anti-bond with the N-O bond but bond to the N-N bond. The LUMO is a 3π*-orbit with anti-bond to the N-O and N-N bond. As in the ^{1}IM1(^{3}IM1), the O-N_1-N_2 system remains linear, but the Cu-O-N_1 angle is bent. These structural parameters can be rationalized by looking at the orbital interactions between the $^1Cu^+(3d^{10}4s^0)$ ion and N_2O, shown in Fig. 3. Apart from a small electrostic and polarized terms, the primary reason for the bent Cu-O-N_1 angle is a σ electron donating interaction between the N_2O HOMO orbit and the $^1Cu^+$ $3dz^2$ empty orbit (Fig. 3a). On the other hand, the interaction between the $^1Cu^+$ 4s orbit and the LUMO orbit of N_2O in-plane, which is lead to the formation of back-donation (Fig. 3b). Additionally, the Cu-O bond length of ^{1}IM1 is shorter than in the excited state Cu-O bond, because of the absence of 4s-ligand repulsion. The molecular orbitals of CO show that the HOMO is a 2σ-orbit which is antibond with the C-O bond (Fig. 3c) and the LUMO is a 2π*-orbit with antibond to the C-O bond (Fig. 3d). As shown in Fig. 4a, the lowest-lying valence orbits of $^3CuO^+(^3\Sigma^-, 2\sigma^2 1\pi^4 1\delta^4 3\sigma^2 2\pi^2 4\sigma^0)$ ion are the

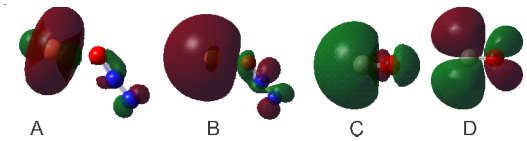

Fig. 3. A. σ [Cu $3d_z^2$-N_2O HOMO-in-plane] interaction, B. σ [Cu 4s-N_2O LUMO-in-plane]. C. CO HOMO. D.CO LUMO

2σ and 1π orbits. The 2π and 1π orbits have significant electron density on both atoms and strong bond. Above these, but very close in energy, lie the non-bond metal-centered 1δ, 3π orbits and the weakly antibond 2π. The lowest-unoccupied molecular orbit (4σ) is mostly antibond. So the LUMO (4σ) of $^3CuO^+$ interact mainly with the CO HOMO (2σ) and the HOMO (2π) of $^3CuO^+$ interact mainly with the CO LUMO (2π*). The result of interaction is that ^{3}IM1 is linear structure. Fig. 4b also shows the lowest-lying valence orbits of $^1CuO^+(^1\Delta, 2\sigma^2 1\pi^4 1\delta^4 3\sigma^2 2\pi^2 2\pi^0)$ ions LUMO (2π) and HOMO (2π) interact mainly with the CO HOMO (2σ) and LUMO (2π*), respectively. The result of interaction is which ^{1}IM2 is curving structure and the angle of C-Cu-^{2}O is 142.2º. According to the above orbital analysis, the conclusion we have drawn is in agreement with the theoretical results which we have calculated.

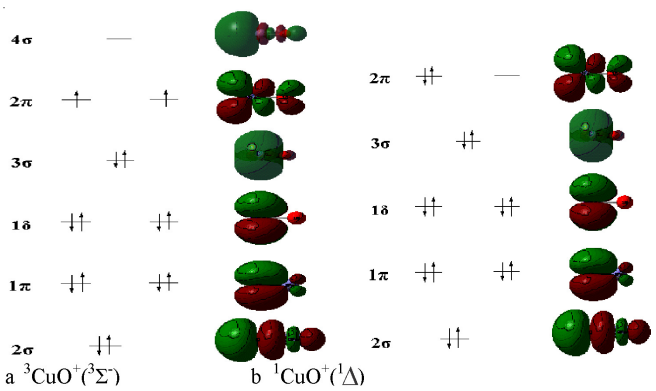

Fig. 4. Molecule orbitals of $^{1\text{-}3}CuO^+$

Charge aspects: To emphasize the importance of charge transfer, the NBO (natural bond orbital) analysis are showed in Table-1 for some key points. The results show that the values of the NBO charge of Cu are from 0.962 (^{1}IM1) to 1.045 (CP1) and then to 1.274 ($^1CuO^+$), from 0.921 (^{3}IM2) to 1.128 (CP2) and then to 0.984 (^{1}IM3). To further understand more detailed information on the net charge transfer (CT) processes can be estimated by second-order perturbation theory ($E(2) = -2 < \sigma|\hat{E}|\sigma^* > /\varepsilon_{\sigma^*}\text{-}\varepsilon_\sigma$)[27]. In the ^{1}IM1, $n_O \rightarrow \sigma_{N_1\text{-}N_2}$ (n_O indicates the lone pair of the O atom, the others are the same means) interaction between the oxygen lone pair and the N_1-N_2 antibond π* orbit is seen to give the strongest stabilization, 33.07 kJ mol^{-1}. In the CP1, the intermolecular CT occurs obviously between the lone pair of O (electron donor) and the Cu antiorbit (electron acceptor) $n_O \rightarrow n^*_{Cu}$, corresponding to the second-order perturbation energies, E(2), 14.40 kJ mol^{-1}. In the ^{3}IM2, $n_{O_2} \rightarrow \sigma^*_{Cu\text{-}N}$ interaction between the second oxygen lone pair and the antibond π* orbit of Cu-N is seen to give the strongest stabilization, 125.1 kJ mol^{-1}. In the CP2, $\sigma_{O_2\text{-}C} \rightarrow n^*_{Cu}$, interaction between the C-O_2 π bond orbit and the atomic empty orbits

TABLE-2
NBO AND ELECTRON CONFIGURATION OF THE Cu ATOM AT THE UB3LYP/6-311+G(2d) LEVEL

Analysis of the second-order perturbation theory						
Species (Cu)	Values of the NBO charge	Electron configuration of Ni	Donor NBO(i)	Acceptor NBO(j)	E(2) kJ/mol	$n_i \rightarrow s^*_j$
^{1}IM1	0.962	$4S^{0.08}3d^{9.95}4p^{0.01}$	LP O	BD*N_1-N_2	33.07	$n_O \rightarrow \sigma^*_{N_1-N_2}$
CP1	1.045	$4S^{0.13}3d^{9.81}4p^{0.01}$	LP O	LP* Cu	14.40	$n_O \rightarrow n^*_{Cu}$
^{3}IM2	0.921	$4S^{0.44}3d^{9.62}4p^{0.01}$	LP O_2	BD* Cu-C	125.10	$n_{O_2} \rightarrow \sigma^*_{Cu-N}$
CP2	1.128	$4S^{0.18}3d^{9.68}4p^{0.02}$	BD O_2-C	LP* Cu	46.23	$\sigma_{O_2-C} \rightarrow n^*_{Cu}$
^{1}IM3	0.984	$4S^{0.06}3d^{9.95}$	LP O_2	BD* O_1-C	412.50	$n_{O_2} \rightarrow \sigma^*_{O_1-C}$

of Cu are seen to give the strongest stabilization, 46.23 kJ mol^{-1}. In the ^{1}IM3, $n_{O_2} \rightarrow \sigma^*_{O_1\text{-}C}$ interaction between the O_2 lone pair and the O_1-C antibond is seen to give the strongest stabilization, 412.5 kJ mol^{-1}. From the NBO analysis, the Cu-O bond is ionic in the $[CuONN]^+$ (IM1) and $[CuOCO]^+$ (IM3) adducts and characterized by a small covalent contribution in the other minima. The most important thing are ^{1}IM1 without ^{1}TS but after CP1 to products N_2 and CuO^+ by scanning bond length of N_1-O and ^{3}IM2 without ^{3}TS2/3 but after CP2 to product complex ^{1}IM3, which means the O has moved to the Cu from the N_2O and the O has moved to the CO from the CuO^+. In the whole cyclic reaction, the Cu^+ is associated with an activation of N_2O and it can be considered as oxygen transfer processes, namely the O atom in N_2O migrates to CO.

Potential surface topology and crossing points: Crossing seams and spin inversion processes are the subject here. Spin inversion is a nonadiabatic process, we need to inspect a crossing seam on the singlet and the triplet potential energy surfaces to know the mechanism of the N_2O ($^1\Sigma^+$) + CO ($^1\Sigma^+$) ⟶ N_2($^1\Sigma_g^+$) + CO_2($^1\Sigma_g^+$) conversion. We performed single-point computations of the singlet state as a function of the structural change along the IRC of the triplet state and vice versa. Such analyses will help us to locate the crossing points. Furthermore, it should be noted that the crossing points obtained in this way could not be considered as the true minimal energy crossing points (MECPs) between two spins state PESs, because when the reaction reaches the vicinity of crossing points, the crossing points in low spin state may mix with that in high spin state that will increase the energy[28].

In Fig. 5a, to obtain CP1, we have attempted to calculate the structure of the singlet-triplet crossing point in the following way: Defining the O-N_1 bond distance as the reaction coordinate, the structure of the singlet state was obtained at several points along the reaction path (the solid lines), by keeping only the latter distance fixed (1 Å) and optimizing all other geometrical parameters. A single-point energy calculation of triplet state was then performed at each of these structures (the dotted lines). As such, CP1 was observed that is about located at S = 6 with a relative energy of 101.8 kJ mol^{-1}. The complex at this point has the C_s geometry and the $^{1\text{-}3}$A′ electronic configuration, which the dissociating N-O bond distance is 1.718 Å and the forming Cu-O bond distance 1.846 Å. In Fig. 5b, the solid lines are the single-point energy values of each optimized point along the IRC paths (2.0 Å) in the triplet state and the dotted lines are the single-point energy values in the singlet state on the geometries of each optimized point along the triplet state

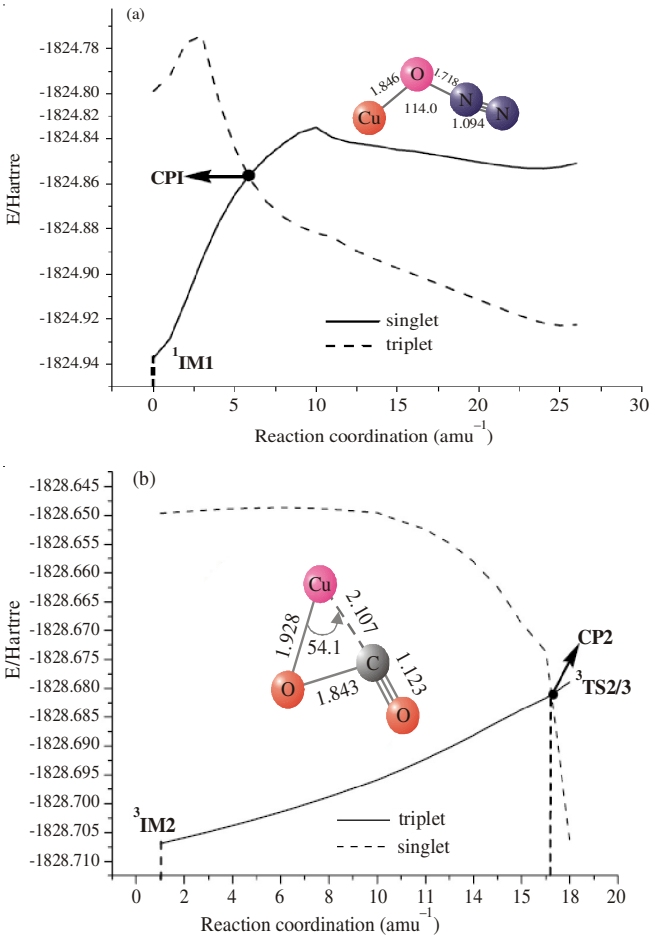

Fig. 5. Potential energies cure-crossing points diagram between two spin state PESs

IRC path. We found that the crossing point CP2 is about located at S = 16 with a relative energy of 3.0 kJ mol^{-1}. The complex at this point has the Cs geometry and the $^{1\text{-}3}$A′ electronic configuration, which the dissociating Cu-O bond distance is 1.928 Å and the forming C-O bond distance 1.843 Å. The singlet and the triplet potential energy surfaces can begin to touch and likely to change its spin multiplicity from the singlet to the triplet states at CP1, then the triplet to the singlet states at the CP2. Appearance of the crossing point CP1 is a very interesting at this crossing region, which does play an essential role and effectively decreased activation energy from 257.6 kJ mol^{-1} to 101.8 kJ mol^{-1}. The crossing point CP2 appears before the transition state $^3TS_{2/3}$ in this crossing region, so it does play an essential role in the entire system of

reaction, by which activation energy can be decreased from 133.3 kJ mol^{-1} to 103.0 kJ mol^{-1} at the entire system. (Note: without Cu^+, the activation energy of entire system of reaction N_2O ($^1\Sigma^+$) + CO ($^1\Sigma^+$) ⟶ N_2($^1\Sigma_g^+$) + CO_2($^1\Sigma_g^+$) is 360.3 kJ mol^{-1}).

Spin-orbit coupling calculation: In fact, as a consequence of a PES lying almost entirely (Fig. 2) below the reaction asymptote, the real energetic expense for the oxide formation decreases considerably with respect to that required in the double case. This means that, the Cu^+ could also be active in catalyzing the reaction. All depends on the probability of the SOC between the double and quartet surfaces at the crossing point. For CP1 and CP2, the computed spin-orbit coupling constants are 630.1 (between ^{1}A and ^{3}A) and 284.2 cm^{-1} (between ^{1}A and ^{3}A), respectively, obtained by using one-electron spin–orbit Hamiltonian in Gamess. As mentioned above, from the crossing points of view of energy and the SOC value, $^1Cu^+ + N_2O + (CO) \rightarrow {}^{1\text{-}3}CP1 \rightarrow {}^3CuO^+ + (N_2) + CO \rightarrow {}^3IM2 \rightarrow {}^{1\text{-}3}CP2 \rightarrow {}^1IM3 \rightarrow {}^1Cu^+ + CO_2 + (N_2)$ minimum reaction pathways are apparently favorable cases for intersystem crossing (ISC). Thus one can assert that the Cu^+ can work as a catalyst thanks to the two state reactivity phenomenon. This result appears to be in slight disagreement with experimental determination[10] despite the conclusions of the ICP/SIFT study, as far as the inactivity of Cu^+ is concerned, are not so categorical.

Summary: A detailed study on the reaction of N_2O ($^1\Sigma^+$) + CO ($^1\Sigma^+$) → N_2($^1\Sigma_g^+$) + CO_2($^1\Sigma_g^+$) catalytic reaction by transition metal ion Cu^+ is reported. From the most stable reactants Cu^+(^{1}S) and ^1N_2O($^1\Sigma^+$) to the most stable products $^1CO_2$($^1\Sigma_g^+$) and $^1Cu^+$(^{1}S), two crossing points(CP1 and CP2) met between reactants and products. The two crossing points are the important aspect in this reaction pathway because spin inversion should occur from the singlet state to the triplet state firstly, then from the triplet state to the singlet state. The reactions of N_2O ($^1\Sigma^+$) + CO ($^1\Sigma^+$) → N_2($^1\Sigma_g^+$) + CO_2($^1\Sigma_g^+$) proceed channel is exothermic by 361.5 kJ mol^{-1} but does not occur directly at room temperature to any measurable extent, because the activation energy of entire system is very high (210.3 kJ mol^{-1}). By the Cu^+, the reaction activation energy can be distinctly decreased from 210.3 kJ mol^{-1} to 101.8 kJ mol^{-1}. The results that we had have shown that N_2O can easy transfer O atom to CO in this catalytic reaction. These theoretical results can provide a guide for further theoretical and experimental researches.

ACKNOWLEDGEMENTS

This work was supported by the Natural Science Foundation of Gansu Province (No. 1208RJZM289).

REFERENCES

1. D.K. Böhme and H. Schwarz, *Angew. Chem. Int. Ed.*, **44**, 2336 (2005).
2. K. Eller and H. Schwarz, *Chem. Rev.*, **91**, 1121 (1991).
3. X. Lif, X.G. Zhang and P.B. Armentrout, *Int. J. Mass Spectrom.*, **255-256**, 279 (2006).
4. Y.C. Tong, Q.Y. Wang, X.J. Xu and Y.C. Wang, *Comput. Theor. Chem.*, **982**, 2 (2012).
5. S. Chiodo, F. Rondinelli, N. Russo and M. Toscano, *J. Chem. Theory Comput.*, **4**, 316 (2008).
6. V. Blagojevic, G. Orlova and D.K. Böhme, *J. Am. Chem. Soc.*, **127**, 3545 (2005).
7. F. Rondinelli, N. Russo and M. Toscano, *Inorg. Chem.*, **46**, 7489 (2007).
8. Y.C. Wang, J.H. Zhang, Z.Y. Geng, D.P. Chen, Z.Y. Liu and X.Y. Yang, *Chem. Phys. Lett.*, **446**, 8 (2007).
9. Y.C. Wang, Q.Y. Wang, Z.Y. Geng, Y.B. Si, J.H. Zhang, H.Z. Li and Q.L. Zhang, *Chem. Phys. Lett.*, **460**, 13 (2008).
10. D.K. Böhme and H. Schwarz, *Angew. Chem. Int. Ed.*, **44**, 2336 (2005).
11. V. Blagojevic, G. Orlova and D.K. Böhme, *J. Am. Chem. Soc.*, **127**, 3545 (2005).
12. V.V. Lavrov, V. Blagojevic, K.K. Gregory, G. Orlova and D.K. Böhme, *J. Phys. Chem. A*, **108**, 5610 (2004).
13. M.J. Frisch, G.W. Trucks, H.B. Schlegel, G.E. Scuseria, M.A. Robb, J.R. Cheeseman, G. Scalmani, V. Barone, B. Mennucci, G.A. Petersson, H. Nakatsuji, M. Caricato, X. Li, H.P. Hratchian, A.F. Izmaylov, J. Bloino, G. Zheng, J.L. Sonnenberg, M. Hada, M. Ehara, K. Toyota, R. Fukuda, J. Hasegawa, M. Ishida, T. Nakajima, Y. Honda, O. Kitao, H. Nakai, T. Vreven, J.A. Montgomery Jr., J.E. Peralta, F. Ogliaro, M. Bearpark, J.J. Heyd, E. Brothers, K.N. Kudin, V.N. Staroverov, R. Kobayashi, J. Normand, K. Raghavachari, A. Rendell, J.C. Burant, S.S. Iyengar, J. Tomasi, M.Cossi, N. Rega, J.M. Millam, M. Klene, J.E. Knox, J.B. Cross, V. Bakken, C. Adamo, J. Jaramillo, R. Gomperts, R.E. Stratmann, O. Yazyev, A.J. Austin, R. Cammi, C. Pomelli, J.W. Ochterski, R.L. Martin, K. Morokuma, V.G. Zakrzewski, G.A. Voth, P. Salvador, J.J. Dannenberg, S. Dapprich, A.D. Daniels, O. Farkas, J.B. Foresman, J.V. Ortiz, J. Cioslowski and D.J. Fox, Gaussian, Inc., Wallingford CT (2009).
14. A.D. Becke, *J. Chem. Phys.*, **98**, 1372 (1993).
15. C. Lee, W. Yang and R.G. Parr, *Phys. Rev. B*, **37**, 785 (1988).
16. S. Gronert, *Chem. Phys. Lett.*, **252**, 415 (1996).
17. C. Gonzalez and H.B. Schlegel, *J. Chem. Phys.*, **90**, 2154 (1989).
18. C. Gonzalez and H.B. Schlegel, *J. Phys. Chem.*, **94**, 5523 (1990).
19. E.D. Glendening, A.E. Reed, J.E. Carpenter and F. Weinhold, NBO 3.0 Program Manual, Madison, WI (1995).
20. C. Heinemann, W. Koch and H. Schwarz, *Chem. Phys. Lett.*, **245**, 509 (1995).
21. K. Yoshizawa, Y. Shiota and T. Yamabe, *J. Chem. Phys.*, **111**, 538 (1999).
22. L. Gracia, L.R. Sambrano, V.S. Safont, M. Calatayud, A. Beltrán and J. Andrés, *J. Phys. Chem. A*, **107**, 3107 (2003).
23. M.W. Schmidt, K.K. Baldridge, J.A. Boatz, S.T. Elbert, M.S. Gordon, J.H. Jensen, S. Koseki, N. Matsunaga, K.A. Nguyen, S. Su, T.L. Windus, M. Dupuis and J.A. Montgomery, *J. Comput. Chem.*, **14**, 1347 (1993).
24. S. Koseki, M.S. Gordon, M.W. Schmidt and N. Matsunaga, *J. Phys. Chem.*, **99**, 12764 (1995).
25. A. Delabie and K. Pierloot, *J. Phys. Chem. A*, **106**, 5679 (2002).
26. V. Blagojevic, G.K. Koyanagi, V.V. Lavrov, G. Orlova and D.K. Bohme, *Chem. Phys. Lett.*, **389**, 303 (2004).
27. Y.C. Wang, D.P. Chen, Z.Y. Geng and J.H. Zhang, *J. Mol. Struct. (Theochem.)*, **855**, 26 (2008).
28. K. Yoshizawa, A. Suzuki and T. Yamabe, *J. Am. Chem. Soc.*, **121**, 5266 (1999).